ISSN 0031-918X, Physics of Metals and Metallography, 2022, Vol. 123, No. 13, pp. 1326–1334. © Pleiades Publishing, Ltd., 2022.
ISSN 0031-918X, Physics of Metals and Metallography, 2022. © Pleiades Publishing, Ltd., 2022.

STRUCTURE, PHASE TRANSFORMATIONS, AND DIFFUSION

Investigation of Thermal and Antimicrobial Properties of NiTiX (X = Ta, Ag, and Nb) Shape Memory Alloys

Yildirim Aydogdu[a, *], Omar Abboosh[b], Pervin Soyer[c], Gökhan Kiliç[d], Asena Savur[e], Fethi Dagdelen[f, **], Ayse Aydogdu[a], and Yagmur Tunali[c]

[a] *Department of Physics, Faculty of Science, Gazi University, Ankara, Turkey*
[b] *Department of Physics, Graduate School of Natural and Applied Sciences, Gazi University, Ankara, Turkey*
[c] *Department of Pharmaceutical Microbiology, Faculty of Pharmacy, Anadolu University, Eskişehir, 26470 Turkey*
[d] *Department of Advanced Techonologies, Graduate School of Natural and Applied Sciences, Gazi University, Ankara Turkey*
[e] *Department of Advanced Techonologies, Graduate School of Natural and Applied Sciences, Ahi Evran University, Kırşehir, Turkey*
[f] *Department of Physics, Faculty of Science, Firat University, Elazığ, Turkey*
**e-mail: y.aydogdu@gazi.edu.tr*
***e-mail: fdagdelen@firat.edu.tr*

Received March 27, 2021; revised October 13, 2021; accepted November 15, 2021

Abstract—In this study, the $Ni_{30}Ti_{50}Ta_{20}$, $Ni_{30}Ti_{50}Ag_{20}$ and $Ni_{29}Ti_{50}Nb_{21}$ shape memory alloys SMAs were produced through the arc-melting method under a high vacuum. The thermal properties and antimicrobial potential for these alloys were investigated. The thermal properties were determined by DSC at different heating rates. According to the DSC results, the austenite phase transformation temperature of $Ni_{30}Ti_{50}Ta_{20}$ alloy is higher than $Ni_{30}Ti_{50}Ag_{20}$ and $Ni_{29}Ti_{50}Nb_{21}$ alloys. The thermal activation energy calculated by Kissinger and Ozawa methods were found as follows: E_a = 156.138 kJ/mol and E_a = 154.37 kJ/mol for $Ni_{30}Ti_{50}Ta_{20}$ alloy, E_a = 124 kJ/mol and E_a = 123.74 kJ/mol for $Ni_{30}Ti_{50}Ag_{20}$ alloy, and E_a = 89.43 kJ/mol and E_a = 90.6 kJ/mol for $Ni_{29}Ti_{50}Nb_{21}$ alloy, respectively. In this study each of alloys exhibited a very strong antifungal ability. When compared by the antibacterial activities; the $Ni_{30}Ti_{50}Ta_{20}$ alloy was showed higher activity than $Ni_{30}Ti_{50}Ag_{20}$ and $Ni_{29}Ti_{50}Nb_{21}$ alloys. It was seen from the Vickers hardness results of the samples that $Ni_{30}Ti_{50}Ta_{20}$ SMA has the highest value. Optical microscope images of the alloys were taken at three different temperatures. Martesite plates were not found in any of the alloys. In addition, no structural changes were observed with the temperature difference. Based on the obtained results, it is suggested that the alloys have a high potential for biomedical applications to prevent bacterial based infections.

Keywords: biomedical, antifungal, NiTi, shape memory alloy, activation energy

DOI: 10.1134/S0031918X21100306

INTRODUCTION

In recent years, materials have played different roles in various fields of life. Nowadays, there are many different types of alloy that are become indispensable for daily life [1]. After the discovery of Nitinol, which was a new type of Shape Memory Alloy (SMA), several companies and scientific research centers are interested in developing and manufacturing smart materials for different purposes such as engineering, medicine, and aerospace. As a result, Nitinol is now widely used in biomedical devices such as dental files, *vena cava* filters, endovascular stents, archwires and guidewires, etc [2].

Biological interactions of some materials change depending on the role assigned and the environment. This has been the highest concern in terms of biology and the benefits of using these materials as biomaterials. The biological impact of materials can be classified into several categories, including carcinogenic, genotoxic, hemotoxic, mutagenic, cytotoxic, and corrosion resistance in a biological environment [3]. Biomaterials used in biomedical devices are an essential component of modern medical therapies and help to improve patients' quality of life [4]. TiNi-based alloys have a wide range of physicochemical properties in a biological environment, making the appropriate for use in biomedical applications. TiNi based biomedical alloys have been extensively used in various clinical applications, including orthodontic therapy, prostheses, catheters, cardiovascular stents, tissue anchoring, and connection [5, 6]. These implanted materials in the body are primary sites for microbial adhesion and microbial contamination, which can lead to the development of critical infections. Novel TiNi alloys with

adding antimicrobial alloying elements become the feasible alternative for clinical needs and applications. The biocompatibility of most of these anti-infective surfaces is still uncertain and needs to be clarified [7]. The Ti, Nb, and Ta are promising elements in biological applications because they are extremely biocompatible [8–10]. Generally, these elements having confirmed with in vitro and in vivo tests [5]. On the other hand, based on different experimental studies, it has been determined that the nickel element has tremendously low biocompatibility with biological side effects. Although a pure nickel element has low biological properties, when used in an alloy can enhance physical properties and can improve its biocompatibility. The alloys are widely used in engineering and biomedical applications. Dagdelen et al. [11] investigated the thermal and microstructure properties of $Ni_{30}Ti_{50}Nb_{20}$ and $Ni_{30}Ti_{50}Ta_{20}$ SMAs. Additionally, Wang et al. investigated the cytotoxicity and hemocompatibility of some TiNb-based SMAs with in-vitro tests [12]. There are many studies on the structural and thermodynamic parameters of NiTiX SMA. However, there is almost no antimicrobial research on these alloys, where the third element (Ta, Nb, Ag) to 20 at % contribution to these alloys has been investigated.

In this study, new SMAs with the nominal composition of $Ni_{30}Ti_{50}Ta_{20}$, $Ni_{29}Ti_{50}Nb_{21}$ and $Ni_{30}Ti_{50}Ag_{20}$ were manufactured under the argon atmosphere by arc melting technique. The physical characteristics such as thermal properties were examined; also, some related calculations were accomplished to explore the thermodynamic properties of the alloys. Also, a comparative study on the antimicrobial potential of different novel TiNi-based SMAs with different antimicrobial methods has been presented.

EXPERIMENTAL PROCEDURE

The elements used in this study are Ni, Ti, Nb, Ta and Ag elements with high purity of at least 99.9%. The metal powders were mixed and formed into small disks (13 mm diameter) under a pressure of 5 MPa. These disks were melted by the arc melting method in a high purity argon atmosphere. The alloy melting processes were repeated several times, then the $Ni_{30}Ti_{50}Ta_{20}$, $Ni_{30}Ti_{50}Ag_{20}$ and $Ni_{29}Ti_{50}Nb_{21}$ polycrystalline alloy ingots were annealed at 850°C for 24 h. The ingots were cooled by very cold water to achieve a high homogeneity. The ingots were cut small unites by a micro cutter. The transformation temperature (TT) and enthalpy change values (ΔH) of martensite and austenite phase transformations were determined by a Differential Scanning Calorimeter (DSC). The mass of samples used in DSC was approximately about 50 mg. DSC measurements of all samples were performed at heating and cooling rates of 10, 15, 20, and 25°C/min under high purity of nitrogen atmosphere. The activation energies were calculated for all alloys. The Vickers microhardness of samples was measured for 10 s under 300 g-force load using Durascan Emcotest 20 model microhardness tester at the room temperature. The average of five measurements taken was evaluated for the microhardness test. Samples for microscopic observation were mechanically polished and chemically etched in a solution of (10 mL HF + 30 mL HNO_3+100 mL pure H_2O) for approximately 5 s. Microstructures were observed by Optical Microscope (OM) (Nikon LV100ND) with heating-cooling system (Linkam THMS600) in martensite and austenite region (at –30, 0, and 150°C) and for cooling liquid nitrogen were used.

The bacteria strains used for this study were *Staphylococcus aureus* ATCC 29213, *Staphylococcus epidermidis* ATCC 14990, *Pseudomonas aeruginosa* ATCC 27853, yeast (fungi) strains *Candida albicans* ATCC 90028, and *Candida krusei* ATCC 6258. Overnight, fresh cultures of the microorganisms were incubated in suitable media; MHA (Mueller Hinton Agar) for bacteria; and SDA (Sabouraud Dextrose Agar) for yeasts. After incubation, McFarland was prepared according to 0.5 standard and the number of microorganisms per millilitres was set to be 1×10^8 for bacteria and 1×10^6 for fungi cultures. Experimental samples of alloys with dimensions of $10 \times 10 \times 1$ mm^3 were sterilized by ultraviolet radiation and placed into 24-well plates. Alloy pellets are coded with $Ni_{30}Ti_{50}Ta_{20}$ (A), $Ni_{30}Ti_{50}Ag_{20}$ (T) and $Ni_{29}Ti_{50}Nb_{21}$ (N). 2 mL of microorganism suspension was then added onto the alloy pellets in the wells. The plates were incubated for 24 h at 37°C. In this test, MHB-SDB media, alloys (without microorganism inoculation), and microorganisms (without alloy samples) were used as control groups. At the end of the incubation period, the samples were washed 3 times with 0.9% NaCl solution to remove microorganisms that have not adhered to the alloy samples. After washing, 2 ml of NaCl solution was transferred to the samples. Afterward, a 500 μL sample was taken from each well and serial dilutions up to 10^{-5} were done in wells that containing 4500 μL 0.9% NaCl solution. 10 μL from the final dilution well was taken and transferred to the previously prepared media of MHA (for bacteria) and SDA (for yeasts) using spread streaking method and incubated at 37°C for 24 h. At the end of the incubation period, the colonies formed on the medium (colony-forming units in millilitres (CFU/mL)) were counted visually and the results were interpreted. The final volume of the wells after transferred for dilution was 1500 mL. The adherent viable microorganism specimens' surfaces were observed by resazurin staining. 150 μL of resazurin stain was added to each well and incubated for an additional 4 h. After 4 h, the results were interpreted according to the color changes in the wells (shades ranging from blue-pink). The experiments were carried out in 3 replications and the average results were obtained [13, 14]. The statistical analyses for quantita-

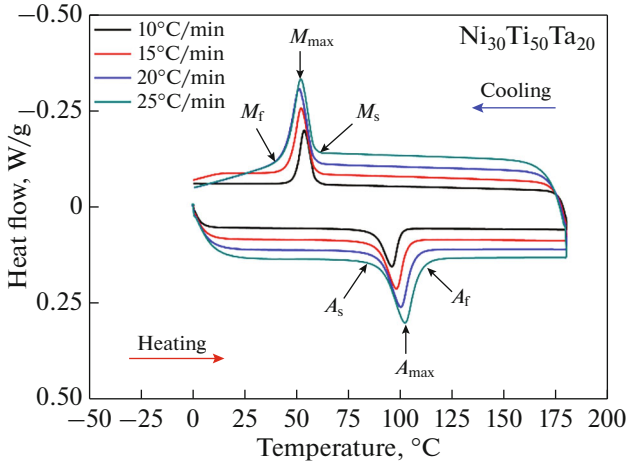

Fig. 1. DSC curves of $Ni_{30}Ti_{50}Ta_{20}$ alloys for different heating/cooling rate.

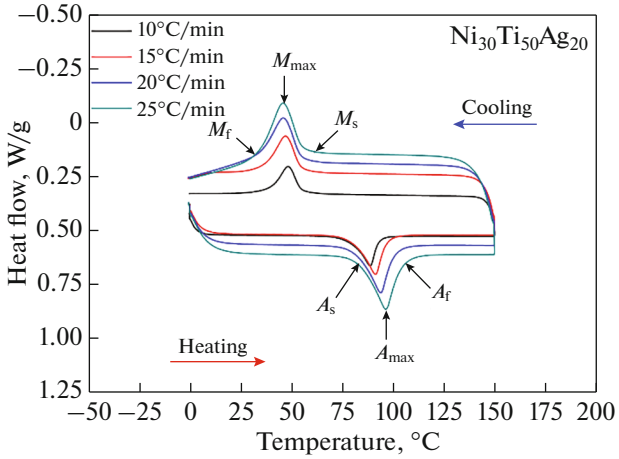

Fig. 2. DSC curves of $Ni_{30}Ti_{50}Ag_{20}$ alloys for different heating/cooling rate.

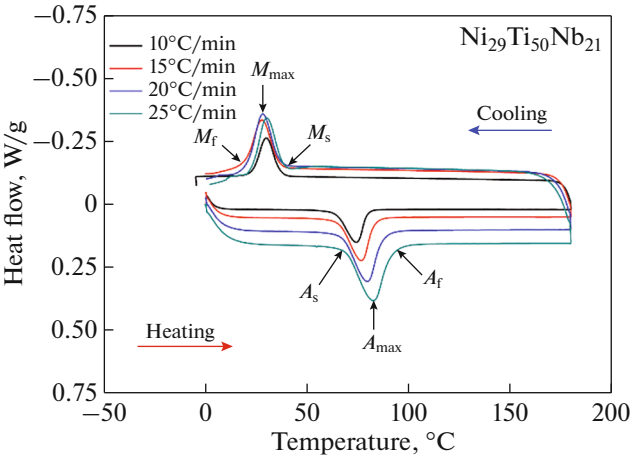

Fig. 3. DSC curves of $Ni_{29}Ti_{50}Nb_{21}$ alloys for different heating/cooling rate.

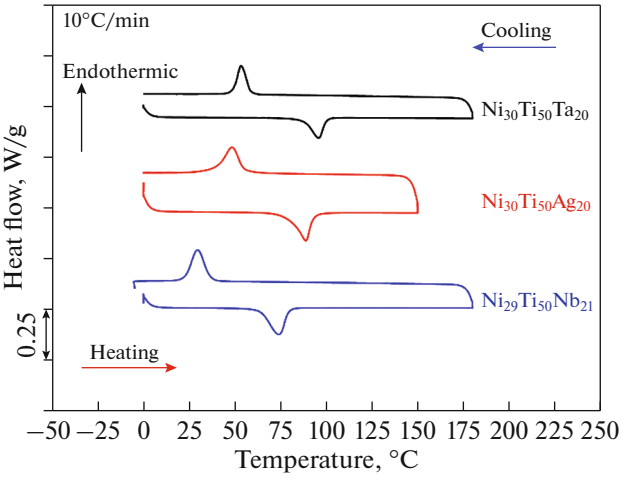

Fig. 4. The DSC curves for $Ni_{30}Ti_{50}Nb_{20}$, $Ni_{30}Ti_{50}Ag_{20}$ and $Ni_{29}Ti_{50}Nb_{21}$ SMAs for heating/cooling rate of 10°C/min.

tive assays were performed using the SPSS 25 software. $P < 0.05$ was considered to be statistically significant.

RESULTS AND DISCUSSIONS

DSC measurements for the heat-treated SMAs were taken with a heating/cooling rate of 10, 15, 20, 25°C/min under 100 mL/min nitrogen gas flow. Figures 1–3 show the behavior of alloys under different heating and cooling rates. The exothermic peaks represent the phase transformation of the alloys from the austenite phase to the martensite phase during cooling. While the endothermic peaks represent the phase transformation from martensite to austenite phase throughout heating. It is found that austenite has a B2 phase with a cubic crystal structure and martensite has B19' phase with a monoclinic crystal structure [8]. The transformation temperatures for phases were determined from the intersections of two tangential lines. Tables 1–3 show the results obtained for different heating and cooling rate. It can be seen that the $Ni_{30}Ti_{50}Ta_{20}$, $Ni_{30}Ti_{50}Ag_{20}$, and $Ni_{29}Ti_{50}Nb_{21}$ SMAs have a different martensitic phase transformation temperatures. The martensite starts (M_s) and finishes (M_f) temperatures of the $Ni_{30}Ti_{50}Ta_{20}$ alloy obtained at 10°C/min were 36.55 and 22.7°C; while the austenite start (A_s) and finish (A_f) during the heating process were 63.83 and 79.35°C, respectively; the value of A_s, A_f, M_s, and M_f of $Ni_{30}Ti_{50}Ag_{20}$ alloy were 79.48, 92.98, 55.28, and 36.22°C obtained for the heating rate of 10°C/min, respectively; similarly, these thermal quantities were equal to 36.55, 22.7, 63.83, and 7 9.35°C for the $Ni_{29}Ti_{50}Nb_{21}$ alloy, respectively. Figure 4 reveals that the $Ni_{30}Ti_{50}Ta_{20}$ alloy has higher TTs for DSC execution at a heating/cooling rate of 10°C/min compared to the $Ni_{30}Ti_{50}Ag_{20}$ and $Ni_{29}Ti_{50}Nb_{21}$ alloys.

Table 1. Transformation temperatures and enthalpies of $Ni_{30}Ti_{50}Ta_{20}$ alloy

Heating rate, °C/min	A_s, °C	A_{max}, °C	A_f, °C	M_s, °C	M_{max}, °C	M_f, °C	ΔH, J/g Heating	ΔH, J/g Cooling
10	87.56	95.66	99.97	58.69	53.42	49.12	5.13	–5.25
15	88.60	98.00	103.28	58.15	51.83	46.18	5.18	–5.56
20	89.60	100.07	106.29	58.29	50.78	43.66	5.17	–7.53
25	90.67	102.17	109.54	58.72	51.53	44.97	5.22	–6.71

Table 2. Transformation temperatures and enthalpies of $Ni_{30}Ti_{50}Ag_{20}$ alloy

Heating rate, °C/min	A_s, °C	A_{max}, °C	A_f, °C	M_s, °C	M_{max}, °C	M_f, °C	ΔH, J/g Heating	ΔH, J/g Cooling
10	79.48	88.75	92.98	55.28	48.56	48.56	7.94	–9.35
15	80.68	91.41	96.76	55.2	47.08	36.22	8.36	–9.28
20	83.13	93.9	100.71	55.94	46.11	32.16	8.61	–13.41
25	83.62	96.58	104.52	57.22	45.68	33.1	8.73	–15.53

Transformation hysteresis H_t is an important factor in SMAs that can remember their original shape. The H_t can be determined by subtracting the austenite finish and martensite start temperatures [15–18]:

$$H_t = A_f - M_s. \quad (1)$$

The H_t of $Ni_{30}Ti_{50}Ta_{20}$, $Ni_{30}Ti_{50}Ag_{20}$, and $Ni_{29}Ti_{50}Nb_{21}$ alloys are 41.28, 37.7 and 42.8°C, respectively. Accordingly, the H_t of $Ni_{30}Ti_{50}Ta_{20}$ SMA is higher than $Ni_{30}Ti_{50}Ag_{20}$ and $Ni_{29}Ti_{50}Nb_{21}$ alloys. The enthalpy changes of $Ni_{30}Ti_{50}Ta_{20}$, $Ni_{30}Ti_{50}Ag_{20}$ and $Ni_{29}Ti_{50}Nb_{21}$ alloys throughout the martensite to the austenite phase transformation ($\Delta H_{M\to A}$) were measured as 5.17, 8.45 and 8.22 J g^{-1}, respectively. The enthalpy change of NiTiAg SMA is higher than NiTiTa and NiTiNb alloys. The transformation hysteresis is unlike the transformation enthalpies for the alloys.

The activation energy (E_a) provides information about the crystallization behavior of SMAs. Different models, including Kissinger and Ozawa's methods, were utilized for calculating the activation energy for the alloys [10, 19–21]. The models are based on the DSC measurements, which were taken for heating rates of 10, 15, 20, and 25°C/min for each sample individually. The Kissinger method is given as follows [22]:

$$\frac{d(\ln(\beta/T_{max}^2))}{d(\ln(1/T_{max}))} = -\frac{E_a}{R} \quad (2)$$

and the Ozawa method can be represented as [23]:

$$\Delta E \cong -2.19R\frac{d\log\beta}{d(1/T_{max})}, \quad (3)$$

where R is the general gas constant ($R = 8.314$ J/mol K), β is the heating rate, and T_{max} is the maximum points of the austenite phase peak. For the Kissinger method, the graph should be between $\ln\left(\beta/T_{max}^2\right)$ and $(1000/T_{max})$, whereas for the Ozawa method it should be between $\log\beta$ and $1000/T_m$. The slope of the linear fitting line in both methods gives the E_a result (Figs. 5, 6). The calculated activation energies for alloys are summarized in Table 4. It's found that the activation energy of $Ni_{30}Ti_{50}Ta_{20}$ alloy is higher than $Ni_{29}Ti_{50}Nb_{21}$ and $Ni_{30}Ti_{50}Ag_{20}$ alloys.

Table 3. Transformation temperatures and enthalpies of $Ni_{29}Ti_{50}Nb_{21}$alloy

Heating rate, °C/min	A_s, °C	A_{max}, °C	A_f, °C	M_s, °C	M_{max}, °C	M_f, °C	ΔH, J/g Heating	ΔH, J/g Cooling
10	63.83	74.01	79.35	36.55	29.52	22.70	8.09	–8.51
15	65.02	74.52	82.73	36.01	27.54	18.98	8.14	–10.10
20	66.17	79.43	87.04	36.52	27.9	20.31	8.31	–9.17
25	68.36	82.2	91.06	37.92	29.91	22.92	8.34	–6.86

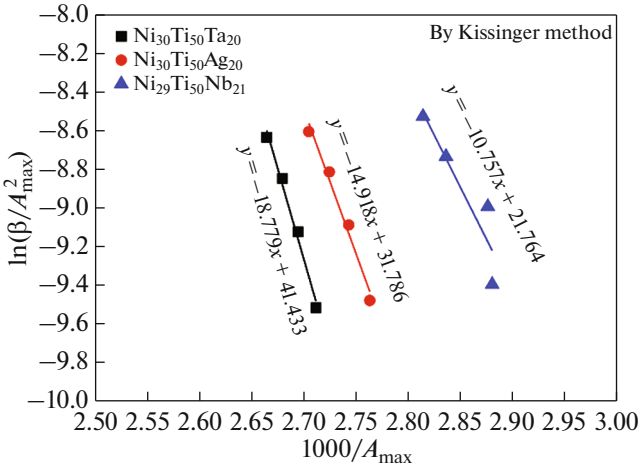

Fig. 5. $\ln(\beta/A_{max}^2)$ versus $1000/A_{max}$ graph to calculate the activation energy of $Ni_{30}Ti_{50}Ta_{20}$, $Ni_{30}Ti_{50}Ag_{20}$ and $Ni_{29}Ti_{50}Nb_{21}$ alloys using the Kissinger method.

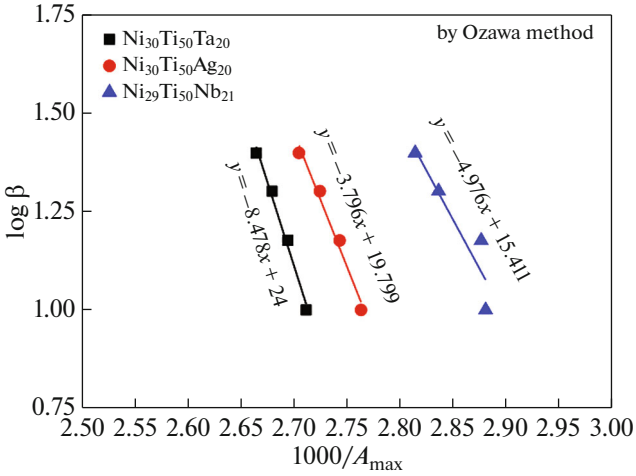

Fig. 6. log(β) vs. $1000/T_{max}$ graph to calculate the activation energy of $Ni_{30}Ti_{50}Ta_{20}$, $Ni_{30}Ti_{50}Ag_{20}$ and $Ni_{29}Ti_{50}Nb_{21}$ alloys by the Ozawa method.

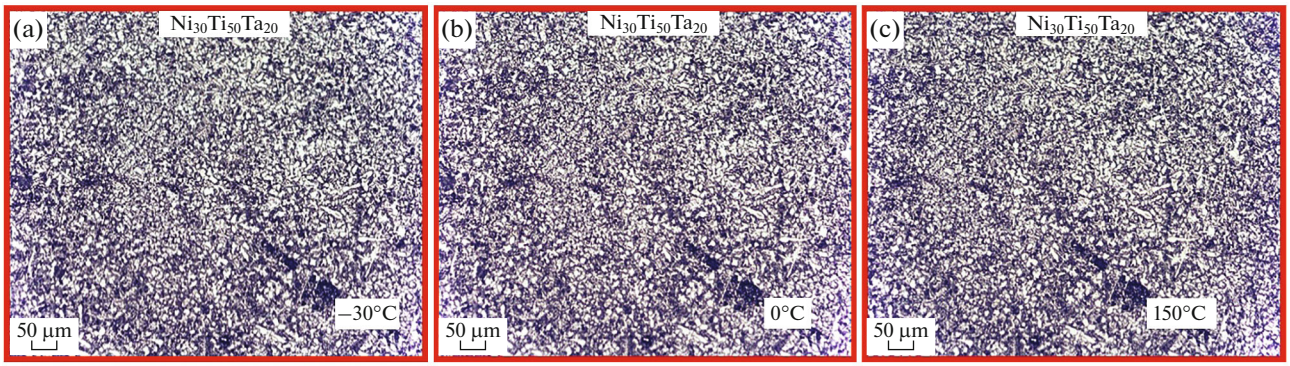

Fig. 7. OM images of the $Ni_{30}Ti_{50}Ta_{20}$ SMA at the different temperature (a) −30, (b) 0, and (c) 150°C.

There are three principal standard test methods for expressing the relationship between hardness. These methods; Vickers, Brinell and Rockwell [24]. In this study, the microhardness test of the shape memory alloys was made using Vickerss hardness measurement method. The micro-hardness values of the NiTiTa, NiTiAg and NiTiNb samples were determined to be 540, 290, and 340 $HV_{0.3}$, respectively. The OM images of the SMAs taken at different temperatures are given in Figs. 7–9. OM image temperatures were selected below the martensite phase (−30°C), above the austenite phase (150°C) and 0°C. Figures 7a–7c shows the microstructure of $Ni_{30}Ti_{50}Ta_{20}$ SMA by means of OM at three different temperatures. It is seen that OM images possess without specific crack. In Fig. 7, dendritic structures and martensite plates are not clearly observed at all temperatures. F. Dagdelen et al. stated that dendrite arms in NiTiTa alloys are Ta-rich structures [11]. It is well known that, with increasing the amount of Ta in the NiTi SMAs, the dendrite lengths increase while random orientations decrease. Also, the length of the binary dendrites will grow. On the other hand, it is well known that the dendritic regions in the NiTiTa SMAs are Ta-rich regions with Ta_2Ni phase, and the main phase is specified to be $(Ti,Ta)_2Ni$ phase and B19' structure [25, 26]. The OM images of NiTiAg

Table 4. The activation energy of the alloys obtained by the Kissinger and Ozawa methods

Alloys	E_a, kJ/mol	
	Kissinger method	Ozawa method
$Ni_{30}Ti_{50}Ta_{20}$	156.138	154.37
$Ni_{30}Ti_{50}Ag_{20}$	124	123.74
$Ni_{29}Ti_{50}Nb_{21}$	89.43	90.6

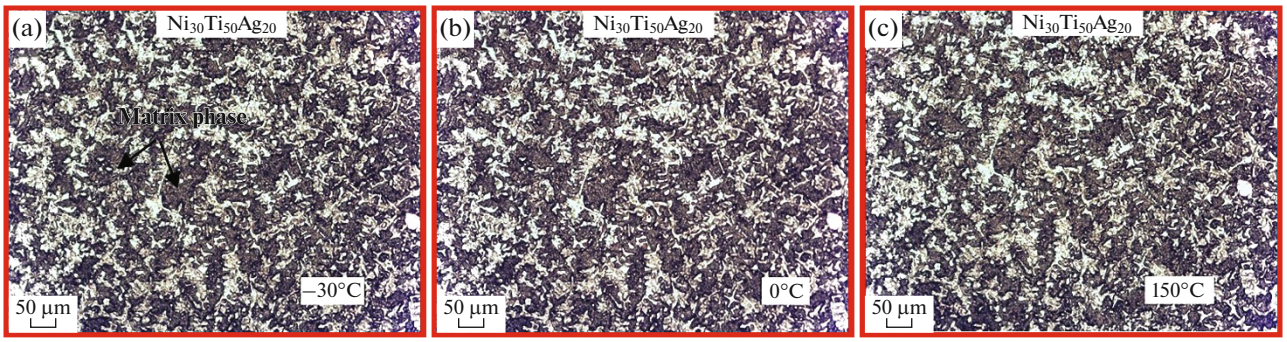

Fig. 8. OM images of the $Ni_{30}Ti_{50}Ag_{20}$ SMA at the different temperature (a) –30, (b) 0, and (c) 150°C.

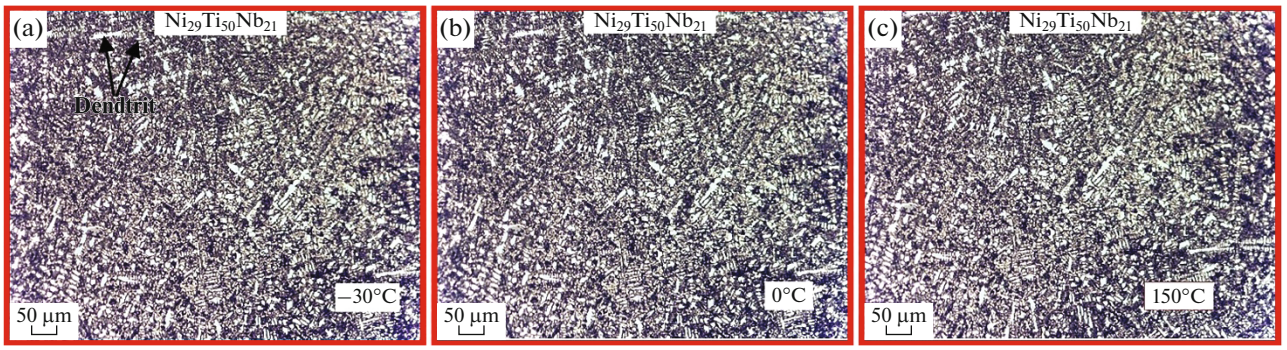

Fig. 9. OM images of the $Ni_{29}Ti_{50}Nb_{21}$ SMA at the different temperature (a) –30, (b) 0, and (c) 150°C.

SMA are given in Fig. 8. It is clear that dendrite arms are not evident, and the grains and martensite plates are not seen in NiTiAg alloy at three different temperatures (Figs. 8a–8c). The matrix phase is clearly seen in Ag added NiTi alloy. In NiTiNb SMA, the primary and secondary dendrite arms are prominent (Figs. 9a–9c). It is clear that the distribution of dendrites has random orientations. In addition, no significant change was observed in the OM images due to temperature change. It has been stated in many studies that dendrite arms in NiTiNb SMA are composed of Nb-rich (β-Nb) structures [27–29].

It is known that the Ti-based alloys exhibited very strong antifungal activity against fungi cells [30, 31]. Table 5 and Fig. 10 show the statistical results of alive *S. aureus, S. epidermidis* and *P. aeruginosa* cells after 24 h incubation, respectively. It can be noted that Ti–Ni–Ta alloys exhibited excellent antibacterial activity to *S. epidermidis* and *P. aeruginosa*. On the contrary, Ti–Ni–Ag showed the poorest antibacterial activities

Table 5. Statistical results of colony counts

Alloys		*S. aureus*	*S. epidermidis*	*P. aeruginosa*
TiNiAg	Mean	207.7000	154.4000	119.0000
	N	10	10	10
	Std. Deviation	4.52278	3.27278	3.01846
TiNiNb	Mean	180.0909	.0000*	42.5455
	N	11	11	11
	Std. Deviation	1.75810	.00000*	1.63485
TiNiTa	Mean	87.5455	42.0000	40.6364
	N	11	11	11
	Std. Deviation	1.91644	5.07937	3.52910
Total	Mean	156.9062	62.6875	65.7813
	N	32	32	32
	Std. Deviation	52.32797	65.35286	36.56610

* .0: All dead. Statistical results indicates the statistically significant differences ($P < 0.05$) when compared with each other.

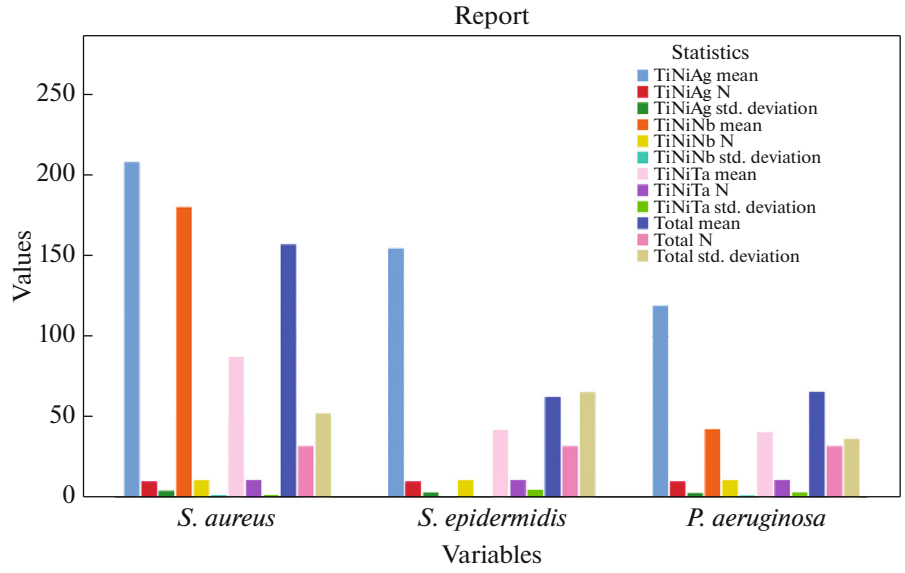

Fig. 10. Statistical results of viable adherent microorganisms.

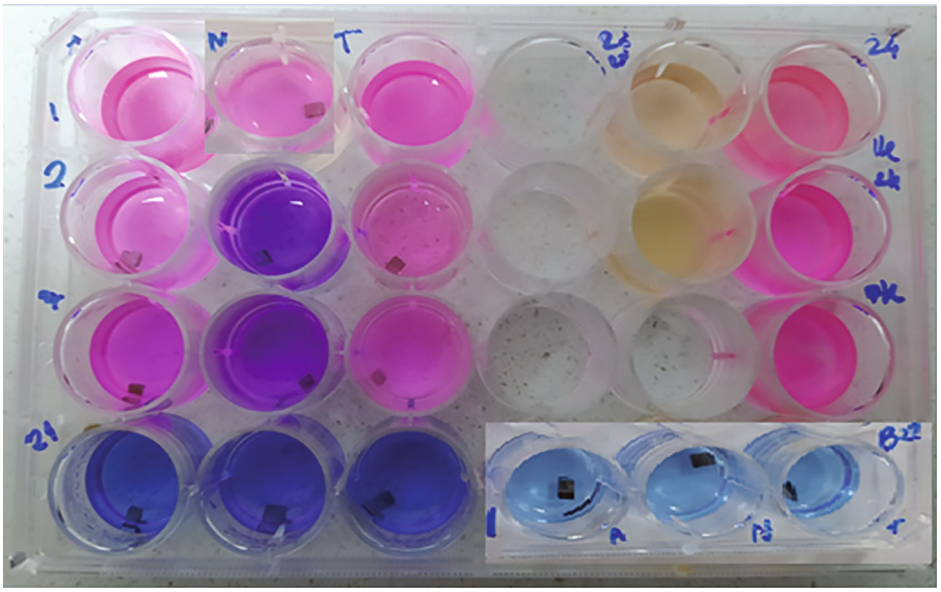

Fig. 11. From left to right are the A, N, T alloys and top to down *Staphylococcus aureus* ATCC 29213, *Staphylococcus epidermidis* ATCC 14990, *Pseudomonas aeruginosa* ATCC 27853 and *Candida albicans* ATCC 90028; and at the right-hand side *Candida krusei* ATCC 6258. * Pink means adherent alive microorganisms in wells, while blue means adherent dead microorganisms.

with the largest number of alive cell counts 24 h incubation. The plate views with alloys and cells are shown in Fig. 11. As a result of tests, all samples are ineffective against the selected test bacteria species (*Staphylococcus aureus* ATCC 29213, *Staphylococcus epidermidis* ATCC 14990, *Pseudomonas aeruginosa* ATCC 27853).

It was observed that only $Ni_{29}Ti_{50}Nb_{21}$(N) alloy had an antibacterial effect against *Staphylococcus epidermidis* ATCC 14990 bacteria. Also, it has been found that alloy samples have a completely antifungal effect against selected yeast (fungi) species (*Candida albicans* ATCC 90028 and *Candida krusei* ATCC 6258) and prevent their growth in the medium. Briefly, $Ni_{30}Ti_{50}Ta_{20}$ (T) exhibited excellent antibacterial properties and the CFU of the alloy was much lower than that of $Ni_{30}Ti_{50}Ag_{20}$ (A), $Ni_{29}Ti_{50}Nb_{21}$ (N) and control groups. $Ni_{30}Ti_{50}Ag_{20}$ (A), $Ni_{30}Ti_{50}Ta_{20}$ (T), $Ni_{29}Ti_{50}Nb_{21}$ (N) alloy samples exhibited more obvious antifungal ability than antibacterial ability since almost no fungal colony remains alive. Consequently, it can be said that

the tested TiNi-based alloy has a toxic effect against eukaryotic cells rather than prokaryotic cells.

CONCLUSIONS

The $Ni_{30}Ti_{50}Ta_{20}$ alloy recorded higher phase transformation temperature (TT) compared to $Ni_{30}Ti_{50}Ag_{20}$ and $Ni_{29}Ti_{50}Nb_{21}$ alloys. The transformation hysteresis (H_t) of $Ni_{29}Ti_{50}Nb_{21}$ alloy was 42.8°C, which was higher than $Ni_{30}Ti_{50}Ta_{20}$ and $Ni_{30}Ti_{50}Ag_{20}$ alloys. The thermal activation energy (E_a) obtained with Kissinger and Ozawa methods were the same for each alloy. It was found that the E_a of the $Ni_{30}Ti_{50}Ta_{20}$ alloy was greater than $Ni_{30}Ti_{50}Ag_{20}$ and $Ni_{29}Ti_{50}Nb_{21}$ alloys. The transformation enthalpy ($\Delta H_{M\to A}$) for $Ni_{29}Ti_{50}Nb_{21}$, $Ni_{30}Ti_{50}Ta_{20}$, $Ni_{30}Ti_{50}Ag_{20}$ alloys were 8.2, 5.17 and 8.45 J/g, respectively. The $Ni_{29}Ti_{50}Nb_{21}$ alloy had the highest transformation enthalpy compared to the other SMAs.

In the current study, we aimed to exhibit the antimicrobial properties of Ni–Ti based alloys via the addition of Ag, Nb, and Ta in order to produce an alloy with good antimicrobial properties. There are very few reports of assessing antimicrobial effects of NiTi-based alloys. Recently, strong antifungal and bacteriostatic effects of Ni–Ti-based alloy composites were shown by this research. As a result of tests, it was observed that our samples have not shown completely antimicrobial effect on selected test bacteria species (*Staphylococcus aureus* ATCC 29213, *Staphylococcus epidermidis* ATCC 14990, *Pseudomonas aeruginosa* ATCC 27853), only NiTiNb (N) alloy showed an effect against *Staphylococcus epidermidis* bacteria because of the differences in growth conditions in the presence of metal ions. It was found that the $Ni_{30}Ti_{50}Ag_{20}$ (A), $Ni_{30}Ti_{50}Ta_{20}$ (T) and $Ni_{29}Ti_{50}Nb_{21}$ (N) alloys were found to exhibit strong antifungal ability against selected yeast (*Candida albicans* ATCC 90028 and *Candida krusei* ATCC 6258). NiTi-based alloys have potential potency to form reactive oxygen species on the cell wall and subsequently damage DNA or proteins. The interaction with cell wall of the pathogens has further accentuated the ability of alloys to the death of the cell walls of the eukaryotic cells. Also, $Ni_{30}Ti_{50}Ta_{20}$ (T) alloy exhibited antibacterial activity properties in comparison with $Ni_{30}Ti_{50}Ag_{20}$ (A) and $Ni_{29}Ti_{50}Nb_{21}$ (N). The possible antibacterial mechanism of Ti–Ni–X alloys; firstly, the X released from alloys, and then enhance the permeability of the bacterial cell membrane, with intracellular material leakage leading to cellular lysis and causes the generation of reactive oxygen species, protein oxidation and DNA degradation in bacteria cells, thus result in the death of bacterial.

The present study introduces, Ti–Ni–X shape memory alloy can be used in order to develop novel antimicrobial ternary alloys. In the light of these data, it can be said that Ti–Ni based alloys tested have toxic effects against eukaryotic cell rather than prokaryotic cell.

FUNDING

This work is supported by TÜBİTAK under Project no. 119M300 and Projects of Scientific Investigation (BAP) Unit of Gazi University under project no. 05/2019-07.

CONFLICT OF INTEREST

The authors declare that they have no conflicts of interest.

REFERENCES

1. F. Dagdelen, M. S. Kanca, and M. Kok, "Effects of Different quenching treatments on thermal properties and microstructure in quaternary Cu-based HTSMA," Phys. Met. Metallogr. **120**, 1378–1383 (2019).
2. J. M. McNaney, V. Imbeni, Y. Jung, P. Papadopoulos, and R. O. Ritchie, "An experimental study of the superelastic effect in a shape-memory Nitinol alloy under biaxial loading," Mech. Mater. **35**, 969–986 (2003).
3. J. Mohd Jani, M. Leary, A. Subic, and M. A. Gibson, "A review of shape memory alloy research, applications and opportunities," Mater. Des. **56**, 1078–1113 (2014).
4. S. S. Mohammed, M. Kok, Z. Cirak, I. Qader., F. Dagdelen, and H. S. A. Zardawi, "The relationship between cobalt amount and oxidation parameters in NiTiCo shape memory alloys," Phys. Met. Metallogr. **121**, 1411–1417 (2020).
5. A. Biesiekierski, J. Wang, M. A-H. Gepreel, and C. Wen, "A new look at biomedical Ti-based shape memory alloys," Acta Biomater. **8**, 1661–1669 (2012).
6. C. L. Chu, R. M. Wang, T. Hu, L. H. Yin, Y. P. Pu, P. H. Lin, S. L. Wu, C. Y. Chung, K. W. K. Yeung, and P. K. Chu, "Surface structure and biomedical properties of chemically polished and electropolished NiTi shape memory alloys," Mater. Sci. Eng., C **28**, 1430–1434 (2008).
7. J. B. Hemmerlein, S. O. Trerotola, M. A. Kraus, M. S. Mendonca, and L. A. Desmomd, "In vitro cytotoxicity of silver-impregnated collagen cuffs designed to decrease infection in tunneled catheters," Radiology **204**, 363–367 (1997).
8. F. Dagdelen, E. Balci, I. N. Qader, E. Ozen, M. Kok, M. S. Kanca, S. S. Abdullah, and S. S. Mohammed, "Influence of the Nb content on the microstructure and phase transformation properties of NiTiNb shape memory alloys," JOM **72**, 1664–1672 (2020).
9. E. Balci, F. Dagdelen, I. N. Qader, and M. Kok, "Effects of substituting Nb with V on thermal analysis and biocompatibility assessment of quaternary NiTiNbV SMA," Eur. Phys. J. Plus **136**, 145 (2021).
10. M. Kök, A. O. Alo Al-Jaf, Z. Deniz Çirak, I. N. Qader, and E. Özen, "Effects of heat treatment temperatures on phase transformation, thermodynamical parameters, crystal microstructure, and electrical resistivity of NiTiV shape memory alloy," J. Therm. Anal. Calorim. **139**, 3405–3413 (2020).

11. F. Dagdelen, and Y. Aydogdu, "Transformation behavior in NiTi–20Ta and NiTi–20Nb SMAs," J. Therm. Anal. Calorim. **136**, 637–642 (2019).
12. B. L. Wang, L. Li, and Y. F. Zheng, "In vitro cytotoxicity and hemocompatibility studies of Ti–Nb, Ti–Nb–Zr and Ti–Nb–Hf biomedical shape memory alloys," Biomed. Mater. **5**, 044102 (2010).
13. H. F. Li, K. J. Qiu, F. Y. Zhou, L. Li, and Y. F. Zheng, "Design and development of novel antibacterial Ti–Ni–Cu shape memory alloys for biomedical application," Sci. Rep. **6**, 37475 (2016).
14. Y. F. Zheng, B. B. Zhang, B. L. Wang, Y. B. Wang, L. Li, Q. B. Yang, and L. S. Cui, "Introduction of antibacterial function into biomedical TiNi shape memory alloy by the addition of element Ag," Acta Biomater. **7**, 2758–2767 (2011).
15. I. N. Qader, E. Öner, M. Kok, S. S. Mohammed, F. Dağdelen, M. S. Kanca, and Y. Aydoğd, "Mechanical and thermal behavior of Cu84–*x*Al13Ni3Hfx shape memory alloys," Iran. J. Sci.Technol., Trans. A: Sci. **45**, 343–349 (2020).
16. I. N. Qader, E. Ercan, B. A. M. Faraj, M. Kok, F. Dagdelen, and Y. Aydogdu, "The Influence of time-dependent aging process on the thermodynamic parameters and microstructures of quaternary Cu79–Al12–Ni4–Nb5 (wt %) shape memory alloy," Iran. J. Sci.Technol., Trans. A: Sci. **44**, 903–910 (2020).
17. E. Acar, M. Kok, and I. N. Qader, "Exploring surface oxidation behavior of NiTi–V alloys," Eur. Phys. J. Plus **135**, 58 (2020).
18. E. Ercan, F. Dagdelen, and I. N. Qader, "Effect of tantalum contents on transformation temperatures, thermal behaviors and microstructure of CuAlTa HTSMAs," J. Therm. Anal. Calorim. **139**, 29–36 (2020).
19. M. Kök, Z. D. Yakinci, A. Aydogdu, and Y. Aydogdu, "Thermal and magnetic properties of Ni51Mn28.5Ga19.5B magnetic-shape-memory alloy," J. Therm. Anal. Calorim. **115**, 555–559 (2014).
20. M. Kök and Y. Aydoğdu, "Effect of composition on the thermal behavior of NiMnGa alloys," J. Therm. Anal. Calorim. **113**, 859–863 (2013).
21. L. V. Spivak and N. E. Shchepina, "Calorimetric effects in the structural and phase transitions of metals and alloys," Phys. Met. Metallogr. **121**, 968–995 (2020).
22. H. E. Kissinger, "Reaction kinetics in differential thermal analysis," Anal. Chem. **29**, 1702–1706 (1957).
23. T. Ozawa, "Kinetic analysis of derivative curves in thermal analysis," J. Therm. Anal. **2**, 301–324 (1970).
24. M. H. Elahinia, *Shape Memory Alloy Actuators: Design, Fabrication, and Experimental Evaluation* (Wiley, New York, 2016).
25. N. Lohan, B. Pricop, M. Popa, E. Matcovschi, N. Cimpoeşu, R. Cimpoeşu, B. Istrate, and L. G. Bujoreanu, "Hot rolling effects on the microstructure and chemical properties of NiTiTa alloys," J. Mater. Eng. Perform. **28**, 7273–7280 (2019).
26. C. Gong, Y. Wang, and D. Yang, "Phase transformation and second phases in ternary Ni–Ti–Ta shape memory alloys," Mater. Chem. Phys. **96**, 183–187 (2006).
27. F. Dagdelen, E. Balci, I. N. Qader, E. Ozen, M. Kok, M. S. Kanca, S. S. Abdullah, and S. S. Mohammed, "Influence of the Nb content on the microstructure and phase transformation properties of NiTiNb shape memory alloys," JOM **72**, 1664–1672 (2020).
28. Q. Fan, M. Y. Sun, Y. H. Zhang, Y. Y. Wang, Y. Zhang, H. B. Peng, K. H. Sun, X. H. Fan, S. K. Huang, and Y. H. Wen, "Influence of precipitation on phase transformation and mechanical properties of Ni-rich NiTiNb alloys," Mater. Charact. **154**, 148–160 (2019).
29. S. Liu, W. Liu, J. Liu, J. Liu, L. Zhang, Y. Tang, L-C. Zhang, and L. Wang, "Compressive properties and microstructure evolution in NiTiNb alloy with mesh eutectic phase," Mater. Sci. Eng., A **801**, 140434 (2021).
30. H. Cao, *Silver Nanoparticles for Antibacterial Devices: Biocompatibility and Toxicity* (CRC Press, 2017)
31. S. A. Fadlallah, N. El-Bagoury, S. M. F. Gad El-Rab, R. A. Ahmed, and G. El-Ousamii, "An overview of NiTi shape memory alloy: corrosion resistance and antibacterial inhibition for dental application," J. Alloys Compd. **583**, 455–464 (2014).